Article:

Brown, N.D. and Rhodes, E.J. orcid.org/0000-0002-0361-8637 (2022) Developing an internally consistent methodology for K-feldspar MAAD TL thermochronology. Radiation Measurements, 153. 106751. ISSN 1350-4487

https://doi.org/10.1016/j.radmeas.2022.106751

Developing an internally consistent methodology for K-feldspar MAAD TL thermochronology

N.D. Brown[a,b,c,*], E.J. Rhodes[b,d]

[a] *Department of Earth and Planetary Science, University of California, Berkeley, CA, USA*
[b] *Department of Earth, Planetary, and Space Sciences, University of California, Los Angeles, CA, USA*
[c] *Department of Earth and Environmental Sciences, University of Texas, Arlington, TX, USA*
[d] *Department of Geography, University of Sheffield, UK*

Abstract

Luminescence thermochronology and thermometry can quantify recent changes in rock exhumation rates and rock surface temperatures, but these methods require accurate determination of several kinetic parameters. For K-feldspar thermoluminescence (TL) glow curves, which comprise overlapping signals of different thermal stability, it is challenging to develop measurements that capture these parameter values. Here, we present multiple-aliquot additive-dose (MAAD) TL dose response and fading measurements from bedrock-extracted K-feldspars. These measurements are compared with Monte Carlo simulations to identify best-fit values for recombination center density (ρ) and activation energy (ΔE). This is done for each dataset separately, and then by combining dose-response and fading misfits to yield more precise ρ and ΔE values consistent with both experiments. Finally, these values are used to estimate the characteristic dose (D_0) of samples. This approach produces kinetic parameter values consistent with comparable studies and results in expected fractional saturation differences between samples.

Keywords: Feldspar thermoluminescence, low-temperature thermochronology, kinetic parameters

*Corresponding author
Email address: nathan.brown@uta.edu (N.D. Brown)

1. Introduction

Recent work has shown that luminescence signals can be used to study the time-temperature history of quartz or feldspar grains within bedrock. Applications include estimations of near-surface exhumation (Herman et al., 2010; King et al., 2016b; Biswas et al., 2018), borehole temperatures (Guralnik et al., 2015b; Brown et al., 2017), and even past rock temperatures at Earth's surface (Biswas et al., 2020). While luminescence thermochronology and thermochronometry provide useful records of recent erosion and temperature changes, these methods depend upon which kinetic model is assumed and how the relevant parameters are determined (cf. Li and Li, 2012; King et al., 2016b; Brown et al., 2017).

In this study, we demonstrate how a multiple-aliquot additive-dose (MAAD) thermoluminescence (TL) protocol can yield internally consistent estimates of recombination center density, ρ (m^{-3}), and activation energy, ΔE (eV), in addition to the other kinetic parameters needed to determine fractional saturation as a function of measurement temperature, $\frac{n}{N}(T)$ (Fig. 1). In MAAD protocols, naturally irradiated aliquots are given an additional laboratory dose before the TL signals are measured. By contrast, the widely used single-aliquot regenerative-dose (SAR) protocol produces a dose-response curve and D_e estimate from individual aliquots which, after the natural measurement, are repeatedly irradiated and measured, each time filling the traps before emptying them during the measurement (Wintle and Murray, 2006). One advantage of a SAR protocol is that each disc yields an independent D_e estimate, which can be measured to optimal resolution by incorporating many dose points. This ensures that with even small amounts of material a date can be determined (e.g., when dating a pottery shard or a target mineral of low natural abundance). The caveat is that any sensitivity changes which occur during a measurement sequence must be accounted for. In optical dating, this is achieved by monitoring the response to some constant 'test dose' administered during every measurement cycle. For TL measurements, however, the initial heating measurement can alter the shape of subsequent regenerative glow curves, rendering this approach of 'stripping out' sensitivity change by monitoring test dose responses as inadequate, because only certain regions within the curve will become more or less sensitive to irradiation (in some cases, this is overcome by monitoring the changes in peak heights through measurement cycles, although this incorporates further assumptions; Adamiec et al., 2006). The MAAD approach avoids such heating-induced sensitivity changes, though radiation-induced sensitivity changes are also possible (Zimmerman, 1971).

2. Samples and instrumentation

The K-feldspar samples analyzed in this study were extracted from bedrock outcrops across the southern San Bernardino Mountains of Southern California. Young apatite (U-Th)/He ages (Spotila et al., 1998, 2001) and catchment-averaged cosmogenic ^{10}Be denudation rates from this region (Binnie et al., 2007, 2010) reveal a landscape which is rapidly eroding in response to transpressional uplift across the San Andreas fault system. Accordingly, we expect the majority of these samples to have cooled rapidly during the latest Pleistocene, maintaining natural trap occupancy below field saturation which is a requirement for luminescence thermochronometry (King et al., 2016a).

Twelve bedrock samples were removed from outcrops using a chisel and hammer. Sample J1298 is a quartz monzonite and the other samples are orthogneisses. After collection, samples were spray-painted with a contrasting color and then broken into smaller pieces under dim amber LED lighting. The sunlight-exposed, outer-surface portions of the bedrock samples were separated from the inner portions. The unexposed inner portions of rock were then gently ground with a pestle and mortar and sieved to isolate the 175 - 400 μm size fraction. These separates were treated with 3% hydrochloric acid and separated by density using lithium metatungstate heavy liquid ($\rho <$ 2.565 g/cm^3; Rhodes 2015) in order to isolate the most potassic feldspar grains. Under a binocular scope, three K-feldspar grains were manually placed into the center of each stainless steel disc for luminescence measurements.

All luminescence measurements were performed at the UCLA luminescence laboratory using a TL-DA-20 Risø automated reader equipped with a ^{90}Sr/^{90}Y beta source which delivers 0.1 Gy/s at the sample location (Bøtter-Jensen et al., 2003). Emissions were detected through a Schott BG3-BG39 filter combination (transmitting between ∼325 - 475 nm). Thermoluminescence measurements were performed in a nitrogen atmosphere.

3. Measurements

To characterize the dose-response characteristics of each sample, 15 aliquots were measured for each of the 12 bedrock samples. Additive doses were: 0 ($n = 6$; natural dose only), 50 ($n = 1$), 100 ($n = 1$), 500 ($n = 1$), 1000 ($n = 3$), and 5000 Gy ($n = 3$). The measurement sequence for each disc is shown in Table 1. Discs were heated from 0 to 500 °C at a rate of 0.5 °C/s to avoid thermal lag between the disc and the mounted grains, with TL intensity recorded at 1 °C increments (Fig. S1).

Thermoluminescence signals following laboratory irradiation (regenerative TL) of K-feldspar samples are known to fade athermally and thermally on laboratory timescales (Wintle, 1973; Riedesel et al., 2021). To quantify this effect in our samples, we prepared 10 natural aliquots per sample. These aliquots were first preheated to 100 °C for 10 s at a rate of 10 °C/s and then heated to 310 °C at a rate of 0.5 °C/s. The preheat treatment is identical to the one used in the dose response experiment described in the additive dose experiment. The second heat is analogous to the subsequent TL glow curve readout (step 3 in Table 1), but the maximum temperature of 310 °C is significantly lower than the peak temperature used in the MAAD dose response experiment. This lower peak temperature was chosen to be just higher than the region of interest within the TL glow curve (150-300 °C), to minimize changes in TL recombination kinetics induced by heating, and ultimately, to evict the natural TL charge population within this measurement temperature range.

Following these initial heatings, aliquots were given a beta dose of 50 Gy, preheated to 100 °C for 10 s at a rate of 10 °C/s and then held at room temperature for a set time (Auclair et al., 2003). Per sample, two aliquots each were stored for times of approximately 3 ks, 10 ks, 2 d, 1 wk and 3 wk. Following storage, aliquots were measured following steps 3 - 8 of Table 1. Typical fading behavior is shown for sample J1499 in Fig. 2 and for all samples in Fig. S2.

4. Extracting kinetic parameters from measurements

To extract kinetic parameters from our measurements, we use the localized transition model of Brown et al. (2017), which assumes first-order trapping and TL emission by excited-state tunneling to the nearest radiative recombination center (Huntley, 2006; Jain et al., 2012; Pagonis et al., 2016). This model is physically plausible, relies on minimal free parameters, and successfully captures the observed dependence of natural TL (NTL) $T_{1/2}$ (measurement temperature at half-maximum intensity for the bulk TL glow curve) on geologic burial temperatures and laboratory preheating experiments (Brown et al., 2017; Pagonis and Brown, 2019). Additionally, the model explains the more subtle decrease in NTL $T_{1/2}$ values with greater geologic dose rates (Brown and Rhodes, 2019) and the lack of regenerative TL (RTL) $T_{1/2}$ variation following a range of laboratory doses (Pagonis et al., 2019).

The kinetic model is expressed as:

$$\frac{dn(r')}{dt} = \frac{\dot{D}}{D_0}\Big(N(r') - n(r')\Big) - n(r')\exp\Big(-\Delta E/k_B T\Big)\frac{P(r')s}{P(r')+s} \tag{1}$$

where $n(r')$ and $N(r')$ are the concentrations (m^{-3}) of occupied and total trapping sites, respectively, at a dimensionless recombination distance r'; $\dot{D}$ is the geologic dose rate (Gy/ka); D_0 is the characteristic dose of saturation (Gy); ΔE is the activation energy difference between the ground- and excited-states (eV); T is the absolute temperature of the sample (K); k_B is the Boltzmann constant (eV/K); and s is the frequency factor (s^{-1}). $P(r')$ is the tunneling probability at some distance r' (s^{-1}):

$$P(r') = P_0 \exp(-\rho'^{-1/3} r') \tag{2}$$

where P_0 is the tunneling frequency factor (s^{-1}). The dimensionless recombination center density, ρ', is defined as

$$\rho' \equiv \frac{4\pi\rho}{3\alpha^3} \tag{3}$$

where ρ is the dimensional recombination center density (m^{-3}). Lastly, α is the potential barrier penetration constant (m^{-1}) (pp. 60-66; Chen and McKeever, 1997):

$$\alpha = \frac{2\sqrt{2m_e^* E_e}}{\hbar} \tag{4}$$

where m_e^* is the effective electron mass within alkali feldspars (kg), estimated by Poolton et al. (2001) as $0.79 \times m_e$; $\hbar$ is the Dirac constant; and E_e is the tunneling barrier (eV), here assumed to be the excited state depth.

In the analyses that follow, we evaluate the dimensional ρ rather than the commonly used dimensionless ρ' to disentangle ρ and ΔE. Within the localized transition model, ρ' embeds depth of the excited state within the tunneling probability term (Eqs. 3 and 4). Assuming a fixed ground-state energy level (Brown and Rhodes, 2017), variation in ρ' then also implies variation in ΔE. Therefore, we isolate these two parameters during data misfit analysis, though we ultimately translate the best-fit ρ into ρ' using the independently optimized ΔE value.

5. Kinetic parameters

We compared results from Eq. 1 with the fading and dose response datasets to estimate the recombination center density ρ (m^{-3}) and the activation energy ΔE of each sample using a Monte

Carlo approach. First, we compared the $T_{1/2}$ values from room temperature fading measurements (Fig. 2) with modeled values produced using Eq. 1 (Fig. 2). For each of the 5000 iterations, values of ρ and ΔE were randomly selected within the ranges of $10^{24} - 10^{28}$ m^{-3} and 0.8 - 1.2 eV, respectively. As illustrated in Fig. 2, higher ΔE values produce less time dependence of $T_{1/2}$ decay and higher ρ values reduce $T_{1/2}$ values at all delay times. Data misfit was quantified with the error weighted sum of squares for all fading durations and the best-fit fifth and tenth percentile contours for these simulations are shown in blue in Fig. 4.

Next, we compared the shape of the MAAD TL curves following the 5 kGy additive dose with that predicted by Eq. 1. Specifically, on a semilog plot of TL intensity versus measurement temperature, the slope of the high-temperature limb of the TL glow curve (defined here as 220 - 300 °C) steepens significantly at greater ρ values, whereas variations in ΔE values produce only slight differences (Fig. 3). Using the same approach and parameter ranges as above, we plot the best-fit fifth and tenth percentile contours in red in Fig. 4. Significantly, the best-fit contours for ρ and ΔE overlap when the fading and curve shape datasets are combined. Values consistent with both the tenth percentile contours of each sample are listed in Table 2.

D_0 values were estimated by comparing measured and simulated TL dose response intensities. Simulated growth curves were produced with Eq. 1, using the best-fit ρ and ΔE values listed in Table 2. We assume that frequency factors P_0 and s equal 3×10^{15} s^{-1} (Huntley, 2006) and the ground-state depth E_g is 2.1 eV (Brown and Rhodes, 2017). Results from 1000 Monte Carlo iterations for sample J1500 are shown in Fig. 5, with the mean and standard deviation of the best-fit fifth percentile values plotted as a red diamond.

Given that all samples are orthogneisses except for J1298, a quartz monzonite, we compare values of derived kinetic parameters (Table 2). Both ΔE and ρ' values are consistent within 1σ. Omitting samples J0165 (1664 $\pm$ 194 Gy) and J1500 (527 $\pm$ 200 Gy), the remaining D_0 values are also consistent within 1σ. Though none of the 12 samples exhibit significantly different properties in hand sample or thin section, sample J1500 comes from a relict surface atop the Yucaipa Ridge tectonic block and is expected to have experienced a higher degree of chemical weathering than any other sample, which may have reduced its D_0 value (cf. Bartz et al., 2022). Alternately, the degree of metamorphism experienced by these rocks prior to exposure at the surface is locally variable (Matti et al., 1992), possibly resulting in different in luminescence properties (Guralnik et al., 2015a).

6. Fractional saturation values

Figure 6 shows the ratio of the natural TL signals to the 'natural + 5 kGy' TL signals. Each ratio shown in Fig. 6 represents the mean and standard deviation of ratios from 6 natural and 3 'natural + 5kGy' aliquots (18 ratios per sample per channel). Ten of 108 aliquots were excluded based on irregular glow curve shapes.

The additive dose responses were corrected for fading during laboratory irradiation, prior to measurement using the kinetic parameters in Table 2 and the approach of Kars et al. (2008), modified for the localized transition model (e.g., Eq. 14 of Jain et al., 2015). Assuming that an additive dose of 5 kGy will fully saturate the source luminescence traps (a reasonable assumption based on the D_0 values in Table 2), these $N/(N + 5$ kGy) ratios are assumed to represent the fractional saturation values for each measurement temperature channel at laboratory dose rates, $\frac{n}{N}(T)$, where $T = 150 - 300$ °C with step sizes of 1 °C. That $\frac{n}{N}(T)$ values of all samples fall within the range of 0 to 1 at 1σ supports this assumption.

Likewise, the differences in $N/(N+5$ kGy) ratios between samples shown in Fig. 6 are expected from their position within the landscape. Sample J0172 ($N/(N + 5 \text{ kGy}) \lesssim 0.2$) is taken from the base of a rocky cliff with abundant evidence of modern rockfall. Sample J0216 ($N/(N + 5 \text{ kGy}) \lesssim 0.4$) is taken from a hillside near the base of the mountains and sample J1502 ($N/(N + 5 \text{ kGy}) \lesssim$

1.0) is taken from a soil-mantled spur. In other words, geomorphic evidence suggests that recent exhumation rates are greatest for sample J0172, less for J0216, and least for J1502. As cooling rate is assumed to scale with exhumation rate, it is encouraging that the calculated $N/(N + 5\text{ kGy})$ ratios for these samples follow this pattern.

7. Conclusions

The kinetic parameters (Table 2) determined using the approach described here and summarized in Fig. 1 are consistent with previous estimates for K-feldspar TL signals in the low-temperature region of the glow curve that assume excited-state tunneling as the primary recombination pathway (Sfampa et al., 2015; Brown et al., 2017; Brown and Rhodes, 2019) as well as numerical results from localized transition models (Jain et al., 2012; Pagonis et al., 2021). Additionally, the ρ and ΔE values determined by data-model misfit of $T_{1/2}$ fading measurements (Fig. 2) and by of glow curve shape measurements (Fig. 3) yield mutually consistent results. By combining these analyses, the best-fit region is considerably reduced, giving more precise estimates of both ρ and ΔE (Fig. 4) which can then be incorporated into the determination of D_0 (Fig. 5). This approach has potential to produce reliable kinetic parameters to better understand the time-temperature history of bedrock K-feldspar samples.

Acknowledgements

We thank Tomas Capaldi, Andreas Lang, Natalia Solomatova and David Sammeth for help with sample collection. We also thank Reza Sohbati for his comments that improved this paper. Brown acknowledges funding by National Science Foundation award number 1806629.

References

Adamiec, G., Bluszcz, A., Bailey, R., Garcia-Talavera, M., 2006. Finding model parameters: Genetic algorithms and the numerical modelling of quartz luminescence. Radiation Measurements 41, 897–902.

Auclair, M., Lamothe, M., Huot, S., 2003. Measurement of anomalous fading for feldspar IRSL using SAR. Radiation Measurements 37, 487–492.

Bartz, M., Peña, J., Grand, S., King, G.E., 2022. Potential impacts of chemical weathering on feldspar luminescence dating properties. Geochronology *Preprint,* DOI: 10.5194/gchron-2022-3.

Binnie, S.A., Phillips, W.M., Summerfield, M.A., Fifield, L.K., 2007. Tectonic uplift, threshold hillslopes, and denudation rates in a developing mountain range. Geology 35, 743–746.

Binnie, S.A., Phillips, W.M., Summerfield, M.A., Fifield, L.K., Spotila, J.A., 2010. Tectonic and climatic controls of denudation rates in active orogens: The San Bernardino Mountains, California. Geomorphology 118, 249–261.

Biswas, R.H., Herman, F., King, G.E., Braun, J., 2018. Thermoluminescence of feldspar as a multi-thermochronometer to constrain the temporal variation of rock exhumation in the recent past. Earth and Planetary Science Letters 495, 56–68.

Biswas, R.H., Herman, F., King, G.E., Lehmann, B., Singhvi, A.K., 2020. Surface paleothermometry using low-temperature thermoluminescence of feldspar. Climate of the Past 16, 2075–2093.

Bøtter-Jensen, L., Andersen, C.E., Duller, G.A.T., Murray, A.S., 2003. Developments in radiation, stimulation and observation facilities in luminescence measurements. Radiation Measurements 37, 535–541.

Brown, N.D., Rhodes, E.J., 2017. Thermoluminescence measurements of trap depth in alkali feldspars extracted from bedrock samples. Radiation Measurements 96, 53–61.

Brown, N.D., Rhodes, E.J., 2019. Dose-rate dependence of natural tl signals from feldspars extracted from bedrock samples. Radiation Measurements 128, 106188.

Brown, N.D., Rhodes, E.J., Harrison, T.M., 2017. Using thermoluminescence signals from feldspars for low-temperature thermochronology. Quaternary Geochronology 42, 31–41.

Chen, R., McKeever, S., 1997. Theory of thermoluminescence and related phenomena. World Scientific.

Guralnik, B., Ankjaergaard, C., Jain, M., Murray, A.S., Muller, A., Walle, M., Lowick, S., Preusser, F., Rhodes, E.J., Wu, T.S., Mathew, G., Herman, F., 2015a. OSL-thermochronometry using bedrock quartz: A note of caution. Quaternary Geochronology 25, 37 – 48.

Guralnik, B., Jain, M., Herman, F., Ankjaergaard, C., Murray, A.S., Valla, P.G., Preusser, F., King, G.E., Chen, R., Lowick, S.E., Kook, M., Rhodes, E.J., 2015b. OSL-thermochronometry of feldspar from the KTB borehole, Germany. Earth and Planetary Science Letters 423, 232 – 243.

Herman, F., Rhodes, E.J., Braun, J., Heiniger, L., 2010. Uniform erosion rates and relief amplitude during glacial cycles in the Southern Alps of New Zealand, as revealed from OSL-thermochronology. Earth and Planetary Science Letters 297, 183–189.

Huntley, D.J., 2006. An explanation of the power-law decay of luminescence. Journal of Physics: Condensed Matter 18, 1359–1365.

Jain, M., Guralnik, B., Andersen, M.T., 2012. Stimulated luminescence emission from localized recombination in randomly distributed defects. Journal of Physics: Condensed Matter 24, 385402.

Jain, M., Sohbati, R., Guralnik, B., Murray, A.S., Kook, M., Lapp, T., Prasad, A.K., Thomsen, K.J., Buylaert, J.P., 2015. Kinetics of infrared stimulated luminescence from feldspars. Radiation Measurements 81, 242–250.

Kars, R., Wallinga, J., Cohen, K., 2008. A new approach towards anomalous fading correction for feldspar IRSL dating–tests on samples in field saturation. Radiation Measurements 43, 786–790.

King, G.E., Guralnik, B., Valla, P.G., Herman, F., 2016a. Trapped-charge thermochronometry and thermometry: A status review. Chemical Geology 446, 3–17.

King, G.E., Herman, F., Lambert, R., Valla, P.G., Guralnik, B., 2016b. Multi-OSL-thermochronometry of feldspar. Quaternary Geochronology 33, 76–87.

Li, B., Li, S.H., 2012. Determining the cooling age using luminescence-thermochronology. Tectonophysics 580, 242–248.

Matti, J.C., Morton, D.M., Cox, B.F., 1992. The San Andreas fault system in the vicinity of the central Transverse Ranges province, Southern California. Open-file report 92-354. US Geological Survey.

Pagonis, V., Ankjaergaard, C., Jain, M., Chithambo, M.L., 2016. Quantitative analysis of time-resolved infrared stimulated luminescence in feldspars. Physica B: Condensed Matter 497, 78–85.

Pagonis, V., Brown, N.D., 2019. On the unchanging shape of thermoluminescence peaks in preheated feldspars: Implications for temperature sensing and thermochronometry. Radiation Measurements 124, 19–28.

Pagonis, V., Brown, N.D., Peng, J., Kitis, G., Polymeris, G.S., 2021. On the deconvolution of promptly measured luminescence signals in feldspars. Journal of Luminescence 239, 118334.

Pagonis, V., Brown, N.D., Polymeris, G.S., Kitis, G., 2019. Comprehensive analysis of thermoluminescence signals in mgb_4o_7:dy,na dosimeter. Journal of Luminescence 213, 334–342.

Poolton, N., Nicholls, J., Bøtter-Jensen, L., Smith, G., Riedi, P., 2001. Observation of free electron cyclotron resonance in $NaAlSi_3O_8$ feldspar: direct determination of the effective electron mass. Physica Status Solidi B 225, 467–475.

Rhodes, E.J., 2015. Dating sediments using potassium feldspar single-grain IRSL: initial methodological considerations. Quaternary International 362, 14–22.

Riedesel, S., Bell, A.M.T., Duller, G.A.T., Finch, A.A., Jain, M., King, G.E., Pearce, N.J., Roberts, H.M., 2021. Exploring sources of variation in thermoluminescence emissions and anomalous fading in alkali feldspars. Radiation Measurements 141, 106541.

Sfampa, I., Polymeris, G., Pagonis, V., Theodosoglou, E., Tsirliganis, N., Kitis, G., 2015. Correlation of basic TL, OSL and IRSL properties of ten K-feldspar samples of various origins. Nuclear Instruments and Methods in Physics Research B 359, 89–98.

Spotila, J., Farley, K., Sieh, K., 1998. Uplift and erosion of the San Bernardino Mountains associated with transpression along the San Andreas fault, California, as constrained by radiogenic helium thermochronometry. Tectonics 17, 360–378.

Spotila, J., Farley, K., Yule, J., Reiners, P., 2001. Near-field transpressive deformation along the San Andreas fault zone in southern California, based on exhumation constrained by (U-Th)/He dating. Journal of Geophysical Research 106, 30909–30922.

Wintle, A., 1973. Anomalous fading of thermoluminescence in mineral samples. Nature 245, 143–144.

Wintle, A., Murray, A., 2006. A review of quartz optically stimulated luminescence characteristics and their relevance in single-aliquot regeneration dating protocols. Radiation Measurements 41, 369–391.

Zimmerman, J., 1971. The radiation-induced increase of the 100C thermoluminescence sensitivity of fired quartz. Journal of Physics C: Solid State Physics 4, 3265–3276.

275 ## Main Text Figures

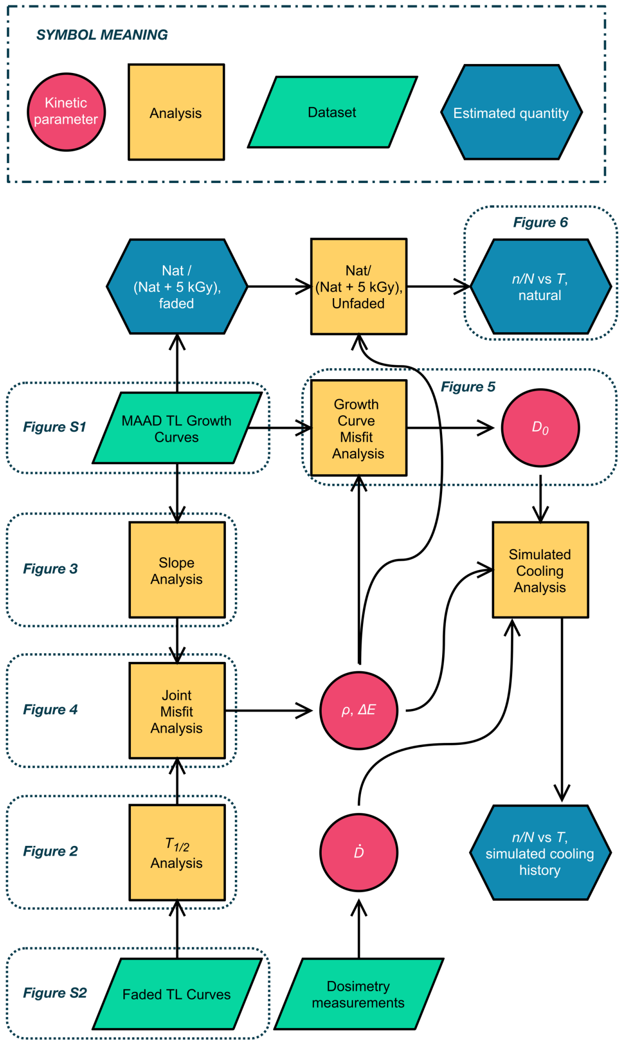

Figure 1: Flowchart illustrating how datasets (green parallelograms) are analyzed (yellow squares) to derive luminescence kinetic parameters (red circles) and other quantities (blue hexagons) to ultimately arrive at fractional saturation as a function of measurement temperature. Figures corresponding to various steps are cross-referenced.

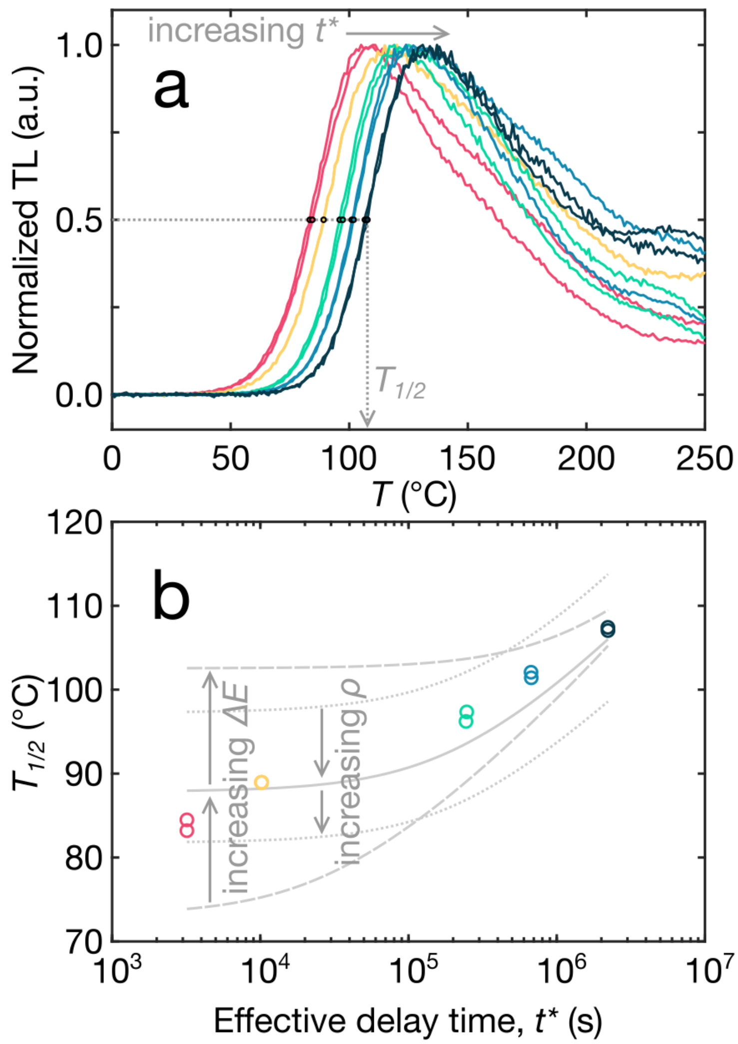

Figure 2: (a) Normalized TL curves of sample J1499 are shown following effective delay times (t^*) ranging from 3197 s (red curves) to 25.7 d (dark blue curves). (b) $T_{1/2}$ values from these glow curves are plotted as a function of t^* (circles). Several simulated datasets are shown for comparison to illustrate the effects of varying luminescence parameters ΔE (values of 1.10, 1.15, and 1.20 eV shown for $\rho = 10^{27.0}$ m^{-3}) and ρ ($10^{26.5}$, $10^{27.0}$, and $10^{27.5}$ m^{-3} shown for $\Delta E = 1.15$ eV).

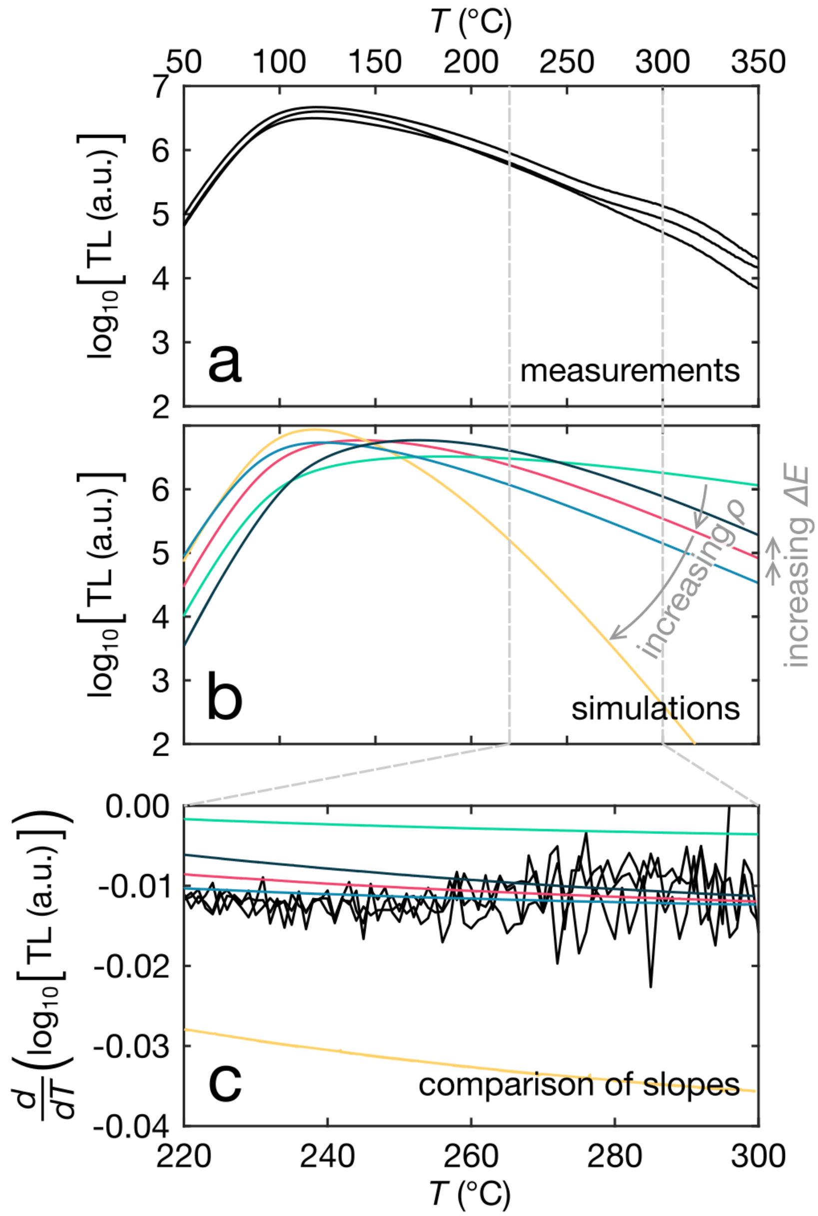

Figure 3: (a) Sensitivity-corrected TL curves for three aliquots of sample J0165 following an additive dose of 5 kGy. The y-axis scaling is logarithmic. (b) Five MAAD TL curves are plotted for comparison to illustrate the effects of varying luminescence parameters ΔE (values of 1.0, 1.1, and 1.2 eV shown for $\rho = 10^{27.0}$ m^{-3}) and ρ ($10^{25.65}$, $10^{26.15}$, and $10^{26.65}$ m^{-3} shown for $\Delta E = 1.1$ eV). (c) The first derivatives of both datasets are plotted together. Note the sensitivity of model fit to ρ value.

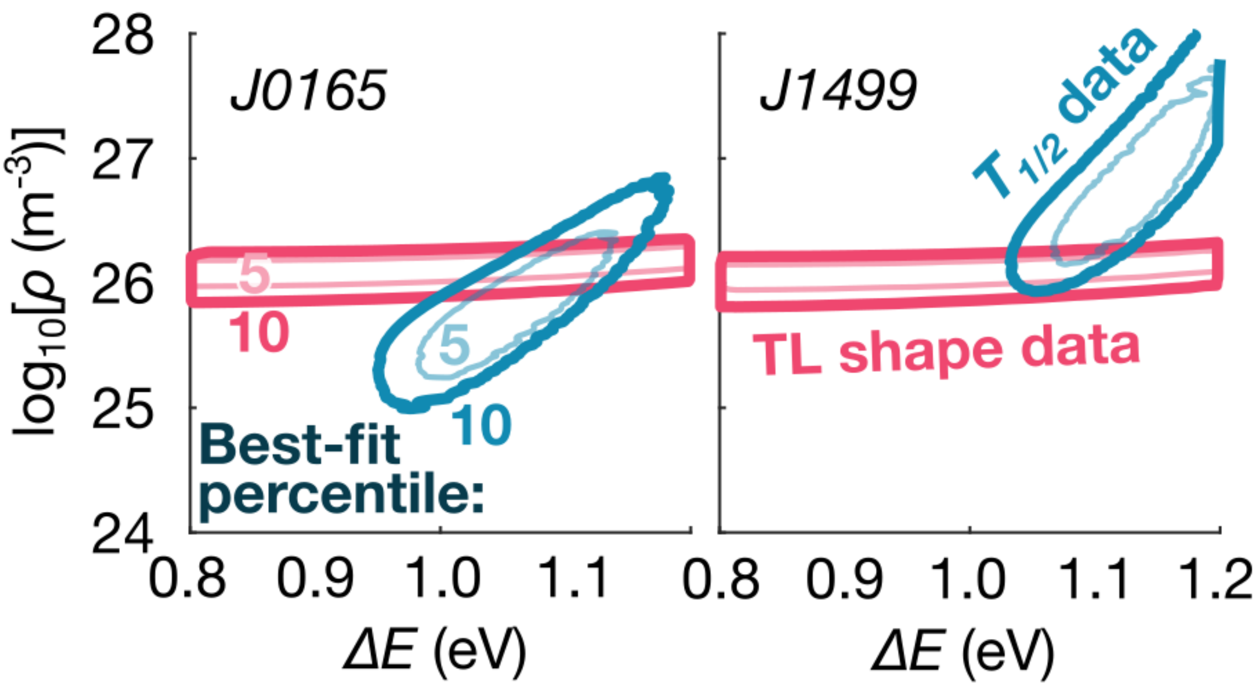

Figure 4: Contours are shown for the 5^{th} and 10^{th} best-fit percentiles of Monte Carlo simulations reproducing TL glow curve shape (red contours) and $T_{1/2}$ dependence on laboratory storage time (blue contours) based upon randomly selected values for parameters ρ and ΔE for samples J0165 and J1499.

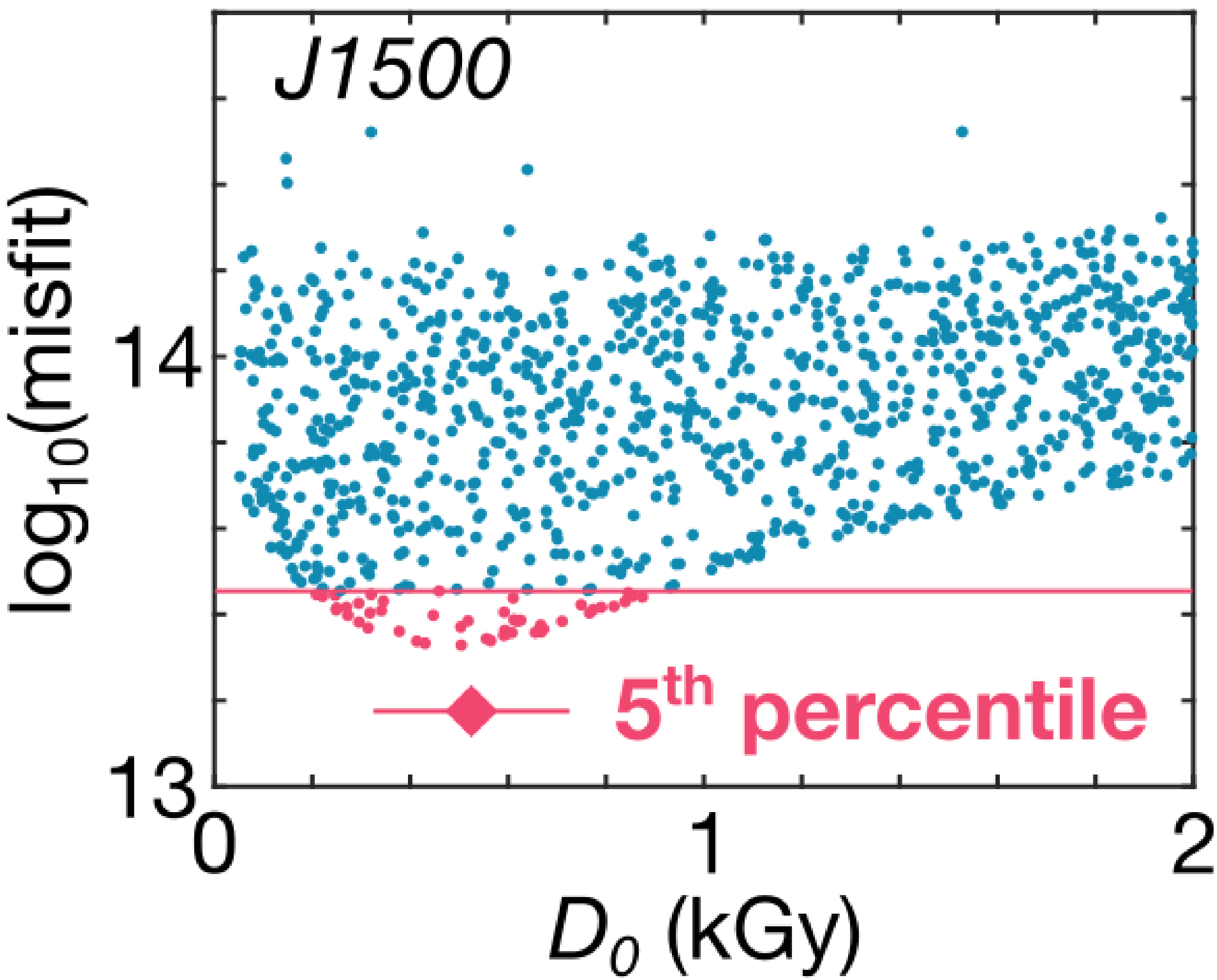

Figure 5: Calculated misfit between measured and simulated TL dose response data as a function of chosen D_0 value, using optimized ρ' and ΔE values listed in Table 2. Monte Carlo iterations from the best-fit 5^{th} percentile (red markers) are used to calculate the D_0, represented by the diamond with error bars and also listed in Table 2.

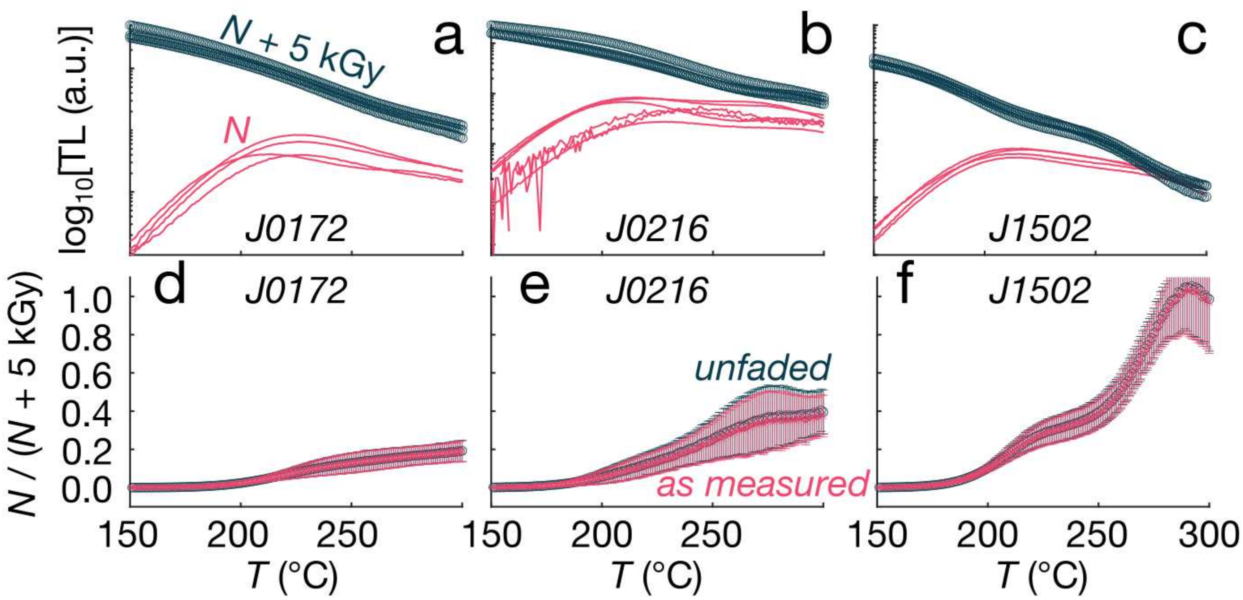

Figure 6: (a - c) The sensitivity-corrected natural (red lines) and 'natural + 5 kGy' (dark blue circles) TL glow curves are shown for samples J0172, J0216, and J1502, with a logarithmic y-axis. Each glow curve is a separate aliquot. (d - f) The 'natural / (natural + 5 kGy)' data are plotted as measured (red Xs) and unfaded (blue circles).

Main Text Tables

Table 1: Thermoluminescence measurement sequence.

Step	Treatment	Purpose
1	Additive dose, $D = 0 - 5000$ Gy	Populate luminescence traps
2	Preheat ($T = 100$ °C, 10 s)	Remove unstable signal
3	TL (0.5 °C/s)	Luminescence intensity, L
4	TL (0.5 °C/s)	Background intensity
5	Test dose, $D_t = 10$ Gy	Constant dose for normalization
6	Preheat ($T = 100$ °C, 10 s)	Remove unstable signal
7	TL (0.5 °C/s)	Test dose intensity, T
8	TL (0.5 °C/s)	Background intensity

Table 2: Thermoluminescence kinetic parameters.

Sample	D_0 (Gy)	ΔE (eV)	$\rho' \times 10^{-4}$
J0165	1664 ± 194	1.08 ± 0.08	7.10 ± 3.94
J0172	1411 ± 318	1.10 ± 0.06	7.65 ± 3.65
J0214	1008 ± 300	1.08 ± 0.08	6.47 ± 3.59
J0216	1097 ± 418	1.04 ± 0.09	5.08 ± 2.69
J0218	936 ± 463	1.04 ± 0.07	5.08 ± 2.42
J1298	1282 ± 328	1.10 ± 0.06	10.57 ± 5.58
J1299	1175 ± 362	1.11 ± 0.07	10.48 ± 5.54
J1300	1006 ± 438	1.09 ± 0.06	7.54 ± 4.18
J1499	932 ± 507	1.08 ± 0.05	6.78 ± 3.23
J1500	527 ± 200	1.09 ± 0.06	7.54 ± 3.99
J1501	959 ± 326	1.11 ± 0.06	10.73 ± 5.67
J1502	1287 ± 325	1.10 ± 0.06	11.32 ± 5.69

Supplementary Figures for 'Developing an internally consistent methodology for K-feldspar MAAD TL thermochronology'

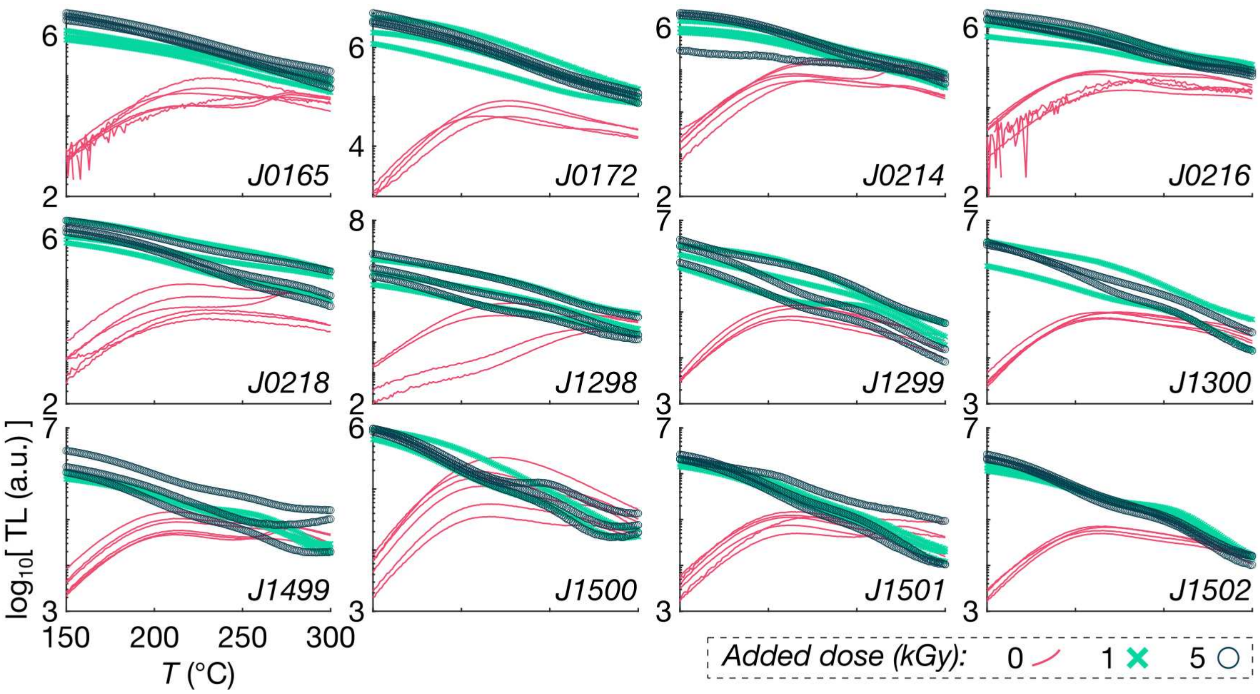

Figure S1: The sensitivity-corrected natural (red curves), 'natural + 1 kGy' (green Xs), and 'natural + 5 kGy' (dark blue circles) TL glow curves are shown for all samples, with a logarithmic y-axis. Each glow curve is a separate aliquot.

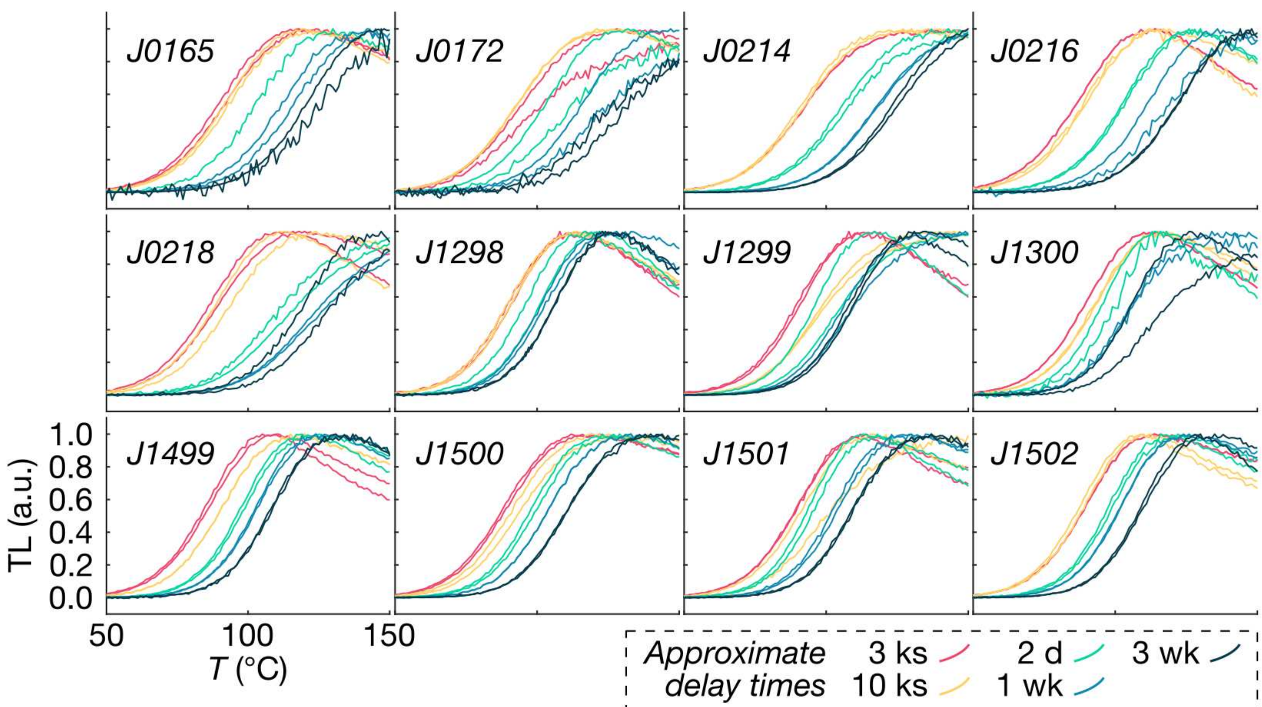

Figure S2: Intensity normalized TL glow curves following a laboratory dose of 50 Gy followed by a preheat and then various room temperature storage durations, ranging from about 3 ks to 3 wk. Each delay time is represented by two aliquots per sample.